Rectification Feedback of High-Frequency Atmospheric Variability into Low-Frequency Zonal Flows in the Tropical Pacific

YOO-GEUN HAM

Global Modeling and Assimilation Office, NASA Goddard Space Flight Center, Greenbelt, and Goddard Earth Sciences Technology and Research Studies and Investigations, Universities Space Research Association, Columbia, Maryland

JONG-SEONG KUG

Korea Ocean Research and Development Institute, Ansan, South Korea

MI-JUNG LIM

School of Earth and Environment Sciences, Seoul National University, Seoul, South Korea

(Manuscript received 21 May 2011, in final form 26 January 2012)

ABSTRACT

In this study, the rectification process of high-frequency (HF) zonal-wind variability on the low-frequency (LF) zonal wind is investigated through an idealized experiment using an atmospheric general circulation model (AGCM). Through an idealized AGCM experiment with a fixed SST boundary forcing, it is shown that there is positive (negative) correlation between HF (2–90-day period) zonal-wind variance and LF (3-month average) zonal wind where the HF zonal-wind variance is positively (negatively) skewed because the stronger HF westerly (easterly) wind events than HF easterly (westerly) wind events induce a residual westerly (easterly), and it results in an additional rectified LF westerly (easterly) anomaly. This means that, over regions with positively skewed HF zonal winds, LF westerly anomalies are generated due to the residuals of the HF zonal winds. It implies that the LF zonal wind can be generated through internal processes of the atmosphere without external forcing and the interaction between LF and HF is not a one-way process from LF to HF but, rather, a two-way interaction process.

1. Introduction

Since the report that the strongest activity of westerly wind events (WWEs) preceded the largest El Niño during 1997–98, numerous studies have suggested the importance of interaction between interannual variability, such as El Niño, and shorter time-scale atmospheric variability, such as the Madden–Julian oscillation (MJO) and WWEs (McPhaden 1999; Moore and Kleeman 1999; Kessler and Kleeman 2000; Vecchi and Harrison 2000; Zhang and Gottschalck 2002; Yu et al. 2003; Kirtman et al. 2005; Wu and Kirtman 2006). Some of these studies noted that the enhanced MJO and WWEs preceded the peak of El Niño by a few months in addition to its simultaneous correlation at the El Niño peak season (Harrison and Schopf 1984; McPhaden et al. 1992, 1998; Fink and Speth 1997; Harrison and Vecchi 1997; McPhaden 1999; Zhang and Gottschalck 2002; Lengaigne et al. 2002; Hendon et al. 2007; Kug et al. 2008a, 2009c,b).

For the strong relationship of WWEs with ENSO, several studies have pointed out that background sea surface temperatures (SSTs) associated with developing ENSO events can modulate the high-frequency (HF) atmospheric variability, suggesting that HF atmospheric variability may be partially deterministic in character (Batstone and Hendon 2005; Eisenman et al. 2005; Vecchi et al. 2006). In addition to the impact of the underlying SST, Sooraj et al. (2009) showed that low-level convergence and horizontal wind shear as well as vertical wind shear is important for modulating the HF wind variability; the HF variability shows maximum increase over the eastern part of the low-frequency (LF) westerly forcing. These findings are consistent with Seiki and Takayabu (2007a,b),

Corresponding author address: Dr. Jong-Seong Kug, Korea Ocean Research and Development Institute, Ansan 435-600, South Korea.
E-mail: jskug@kordi.re.kr

DOI: 10.1175/JCLI-D-11-00303.1

© 2012 American Meteorological Society

who showed that WWEs tended to occur frequently under LF environmental westerlies by analyzing the eddy kinetic energy (EKE) budget. This HF atmospheric variability, which depends on a slowly varying LF state, is often denoted as ''state dependent'' or ''multiplicative'' noise (Blaauboer et al. 1982; Timmermann and Lohmann 2000; Jin et al. 2007; Kug et al. 2008a).

Meanwhile, many studies have argued that HF atmospheric variability can trigger and/or amplify ENSO (Kessler and Kleeman 2000; Shinoda and Hendon 2002; Lengaigne et al. 2004; Eisenman et al. 2005; Perez et al. 2005; Zavala-Garay et al. 2005; Gebbie et al. 2007; Jin et al. 2007). Among them, some assumed the HF variability as an additive noise; therefore, modulation of HF activity can modulate interannual frequencies through nonlinear responses of oceanic processes. In this view, HF atmospheric variability is a random process, independent of the slowly varying large-scale features such as SST. For example, Kessler and Kleeman (2000) argued that nonlinear responses of evaporation, equatorial zonal currents, and vertical advection to a linear HF atmospheric forcing can induce the rectified warming related to El Niño. Han et al. (2004) mentioned that the major nonlinear processes that determine rectified surface currents are an asymmetric response of the mixed-layer depth to zonal winds, upwelling, and entrainment of subsurface water into the surface layer. Similarly, LF shoaling of the mixed layer depth appears to be associated with the basic nonlinear aspect of the mixed layer—that a given positive heat flux anomaly into the ocean, resulting in ocean heating, is typically more effective at shoaling the mixed layer depth than a negative anomaly is at deepening it (Kraus and Turner 1967; Waliser et al. 2003).

Expanding on these early works, recent studies have argued that the interaction between ENSO and the HF atmospheric variability, which modulates not only ENSO instability but also ENSO asymmetry, can be modeled as a state-dependent or multiplicative noise forcing. For instance, Jin et al. (2007) demonstrated in a conceptual framework that state-dependent or multiplicative noise forcing enhances ENSO instability and its ensemble spread and thus generates ENSO asymmetry. In addition, Gebbie et al. (2007) found that the modulation of WWEs by SST strongly affected the characteristics of ENSO in a hybrid coupled model. In particular, coupled feedbacks between SST and WWEs may be sufficient to transform the system from a damped regime to one with self-sustained oscillations.

In addition, the asymmetry of a HF anomaly can lead to the rectification of HF variance in a LF anomaly. Until now, this is only shown and argued mainly for decadal variability over the Pacific caused by asymmetry of the ENSO (Timmermann et al. 2003; Jin et al. 2003; Rodgers et al. 2004; An et al. 2005; An et al. 2008). For example, An et al. (2005) showed that decadal changes in the skewness and variance of model-simulated ENSO SST and nonlinear dynamical heating, which lead to ENSO asymmetry, are highly correlated with the decadal variation in tropical SST. Similarly, this mechanism can be applied to the interaction between HF zonal-wind variability and LF zonal winds because easterly wind events (EWEs) are rarely observed relative to WWEs, possibly due to nonlinear precipitation processes (Kug et al. 2010c). This may change the LF zonal-wind anomaly of the atmospheric circulation by its residual components (Zavala-Garay et al. 2005). In this case, HF zonal-wind variability can directly affect ENSO by altering LF zonal winds. This process is called the ''rectification process.''

Despite this intuitive speculation, so far the rectification feedback of HF zonal-wind variability has not been investigated extensively. Therefore, in this study the impact of HF zonal-wind variability on the generation of LF zonal winds is investigated using an atmospheric general circulation model (AGCM). Following the terminology of Kug et al. (2010c), the generation process of residual LF zonal wind by HF zonal-wind variance is defined as the rectification process in this study.

The paper is organized as follows. In section 2, we describe the AGCM used in this study, datasets used, and the experimental design. In section 3, rectification of HF zonal-wind variability in the LF zonal winds is explained. A summary and discussion are included in section 4.

2. Model, experimental design, and data

a. Model

The model used in this study is the Seoul National University AGCM (SNU AGCM). It is a global spectral model at T42 resolution with 20 vertical sigma levels. The deep convection scheme is a simplified version of the relaxed Arakawa–Schubert scheme (SAS) (Numaguti et al. 1995). The large-scale condensation scheme consists of a prognostic microphysics parameterization for total cloud liquid water (Le Treut and Li 1991) with a diagnostic cloud fraction parameterization. A nonprecipitating shallow convection scheme (Tiedtke 1983) is also implemented in the model for the midtropospheric moist convection. The boundary layer scheme is a nonlocal diffusion scheme based on Holtslag and Boville (1993), while the land surface model is from Bonan (1996). Atmospheric radiation is parameterized by a two-stream k distribution scheme as in Nakajima et al. (1995). In addition, in this study the cumulus momentum transport (CMT) parameterization suggested

by Wu and Yanai (1994) is implemented. Other details of the model physics are described in Lee et al. (2001, 2003) and Kim et al. (2008). Model performance on the climate simulation is referred to in Kug et al. (2008b).

b. Data

The daily- and monthly-mean winds are obtained from the National Centers for Environmental Prediction–National Center for Atmospheric Research (NCEP–NCAR) reanalysis (Kalnay et al. 1996). SSTs are from the NOAA Extended Reconstructed Sea Surface Temperature (ERSST) (Smith and Reynolds 2003). For the observed rainfall we use the 1979–2004 monthly mean data from the Climate Prediction Center Merged Analysis of Precipitation (CMAP) (Xie and Arkin 1997). In addition, daily mean precipitation from 1979 to 2005 is obtained from the Global Precipitation Climatology Project (GPCP) (Huffman et al. 2001).

c. Experimental design

In this study, we focus on the winter season of December–February (DJF) and use a prescribed SST as a boundary condition, averaged for the DJF season, and perpetual solar irradiance, at the equinox, with a solar constant of 1365 W m^{-2}, for the distribution of insolation at the top of the atmosphere. Note that seasonality of the AGCM simulation is mostly dependent on the SST forcing, not the irradiance, because the irradiance is transmitted through the atmosphere and then directly absorbed by the ocean. It means the impact of the irradiance is can be ignored over the ocean when the SST forcing is fixed, even though it can cause a different equilibrium state over land due to air–land coupling.

One may ask why we focused on the DJF season since the westerly wind burst related to the ENSO peaks several months prior to the DJF season (Hendon et al. 2007; Kug et al. 2008a). Since these studies focused on the relation between ENSO SST anomalies and HF zonal-wind variance, we selected the DJF season because the relationship between the LF zonal wind and HF zonal-wind variance over the tropical Pacific is most clear during this season. According to Kug et al. (2009c), the relation between LF wind and HF wind variance is strongest over the central Pacific during the ENSO peak phase, while the relation is a bit weaker during the ENSO developing phase. Kug et al. also showed that, in the experiments with SNU AGCM, the LF–HF relationship is well simulated during ENSO peak phase, while during ENSO developing phase the model has a problem in simulating the observed relationship. In addition, the HF zonal-wind variance over the equatorial region and Southern Hemisphere is also strongest during the DJF season (not shown), which possibly leads to a strong rectification process. This perpetual experiment is advantageous for investigating internally generated atmospheric variability because the SST forcing is fixed in time. If SST forcing is varying in time, it would generate SST-forced LF wind variability and become confused with LF winds generated by atmospheric internal processes. This may prevent clear separation of internally generated LF wind from SST-forced LF wind.

In this study, we performed two sets of AGCM simulations: one with climatological SST and the other with El Niño SST. The AGCM simulation whose SST boundary condition is the climatological SST (El Niño SST) is denoted as CliSST (ElSST). The SST forcing of CliSST is obtained from the DJF climatology averaged from 1981 to 2008 of ERSST. The SST boundary condition of the ElSST run is obtained from the composite for El Niño events during the DJF season as follows. We select five El Niño events whose magnitude of the Niño-3.4 index during DJF is largest, which include events from the DJF season of 1982/83, 1986/87, 1991/92, 1994/95, and 1997/98, and positive SST anomalies over the Pacific (15°S–15°N, 120°E–90°W) are added to the climatological SST of the CliSST run to obtain SST forcing for the ElSST run. Each AGCM simulation is integrated for 30 years. Recently, several studies reported that there are two types of El Niño events, whose spatial patterns are considerably different (Ashok et al. 2007; Kao and Yu 2009; Kug et al. 2009a). In addition to the spatial pattern, their dynamics and teleconnections are somewhat different (Weng et al. 2007; Kug et al. 2010b,a; Kug and Ham 2011). It is possible that the rectification feedback of HF wind variability can be dependent on the type of El Niño. For simplicity, however, we did not consider two types of El Niño by selecting El Niño events based on the single Niño-3.4 SST because our main focus is on the atmospheric internal process independent of the external SST forcings.

To define the HF zonal wind, a 2–90-day Lanczos bandpass filter (using 45 weights, Duchon 1979) is applied to the daily-mean zonal-wind anomalies at 850 hPa. Note that the period 2–90 days (or similar to this period) is used because the MJO variability, having the longest time scale among all equatorial waves, has 30–90-day periods. This criterion with 90 days is also used in several studies to retain the HF components (Kug et al. 2009c; Kim et al. 2009). To check the realism of simulated convectively coupled waves over the tropics, we followed the method of Wheeler and Kiladis (1999). Figure 1 shows symmetric and antisymmetric raw spectra of precipitation and zonal wind at 850 hPa divided by the background spectra in observations and the CliSST run. Dispersion curves are obtained using the theoretical signal of Kelvin, equatorial Rossby (ER), and westward inertia–gravity (WIG) waves in the symmetric spectra of the mixed Rossby–gravity

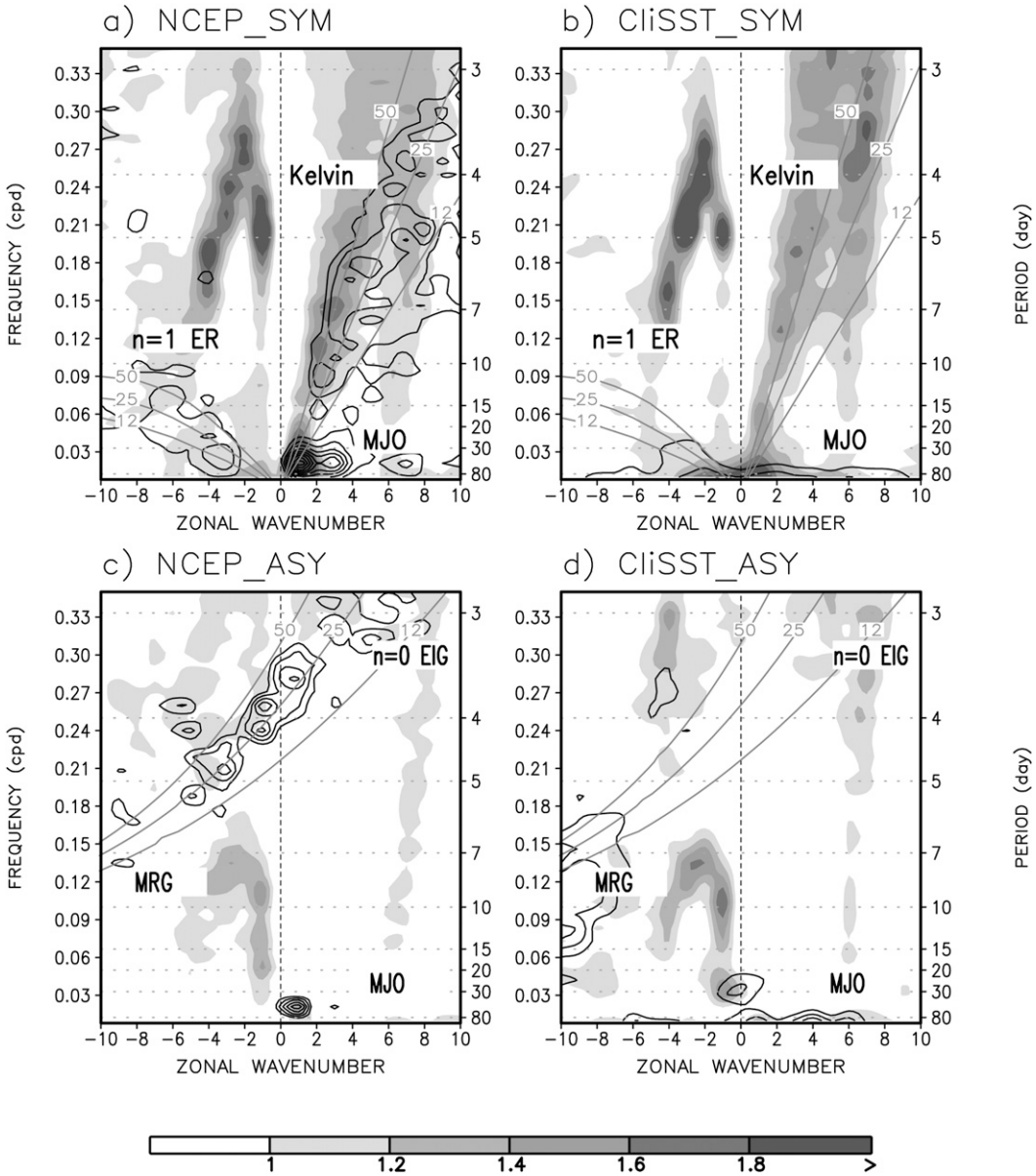

FIG. 1. Space–time spectrum of the daily-mean zonal wind at 850 hPa (shading) and precipitation (contours) divided by the background spectrum in the (left) observations and (right) CliSST run. The top (bottom) panels are of symmetric (antisymmetric) component. Superimposed are the dispersion curves of the meridional mode odd-numbered equatorial waves for equivalent depths 12, 25, and 50 m. Note that the GPCP output from 1979 to 2005 is used as observational precipitation.

(MRG) and eastward intertia–gravity (EIG) waves in the antisymmetric spectra. Note that the waves with period shorter than 90 days are shown to investigate the HF components in the observations and model simulation. In the power spectrum of the low-level zonal wind, the eastward-propagating MJO component, whose period is between 30 and 90 days, and the eastward-propagating Kelvin wave component are clearly shown in both the observations and model simulation. However, the signal of the eastward-propagating MJO is weaker in the model simulation than observed (Lin et al. 2006). In addition, there is a spectral peak at westward wavenumbers 1–8 with period 3–10 days, known as the Rossby–Haurwitz wave, that is detected in both the observations and model simulation (Hendon and Wheeler 2008). The power spectrum of precipitation in the observations shows a similar spectral peak to that in zonal wind except for the westward-propagating equatorial Rossby

wave. This equatorial Rossby wave signal is not well simulated in the CliSST run.

The low frequency modulation of the HF zonal-wind variance is defined by calculating the averaged variance of the HF wind for three months (e.g., four outputs per year). For example, the first season is a 3-month averaged value from the first to third month. Similarly, the second season is a 3-month average from the fourth to sixth month. Hereafter, the variance of the high-pass filtered zonal-wind anomaly averaged for three months is denoted as the ''HF zonal-wind variance.'' Similarly, the 3-month averaged zonal wind is defined as the ''LF zonal wind.''

3. Results

Prior to examining model results, we first show some observational features of the LF fields and HF zonal-wind variability during El Niño events. Figure 2 shows SST, zonal wind at 850 hPa, precipitation anomalies, and anomalous HF zonal-wind variance during boreal winter (December–February) of the selected El Niño events. Note that five El Niño events, which include1982–83, 1986–87, 1991–92, 1994–95, and 1997–98, are selected for the El Niño composite as done for obtaining the prescribed SST for the ElSST run. The anomalous HF zonal-wind variance is calculated by subtracting the averaged variance of DJF HF zonal wind during the selected El Niño years from that during the DJF seasons of all years from 1979 to 2005. As is well known, the positive SST anomaly of the eastern equatorial Pacific associated with El Niño events is often accompanied by an overlying westerly wind and positive precipitation anomalies. In addition, the enhanced HF zonal-wind variance is seen east of 180° where the LF zonal-wind anomaly is strong. On the other hand, weaker HF zonal-wind variance is observed between 150°E and 180°.

These results are consistent with several studies on modulation of HF zonal-wind variability during El Niño (Kessler et al. 1995; Lau and Lau 1992; Hendon et al. 2007; Kug et al. 2009c; Sooraj et al. 2009). For example, Hendon et al. (2007) and Kug et al. (2009c) showed that the HF zonal-wind variance is enhanced (reduced) over the central (western) Pacific during the El Niño peak phase. They also concluded that an eastward extension of the warm pool and enhanced LF westerlies can accompany the eastward expansion of strong MJO activity and WWEs during the El Niño mature phase. In addition, Seiki and Takayabu (2007b) suggested a mechanism of WWE development by performing a budget analysis using an EKE equation. They found that the strength of WWEs was dominated generally by the barotropic energy conversion terms, which are related to the zonal convergence

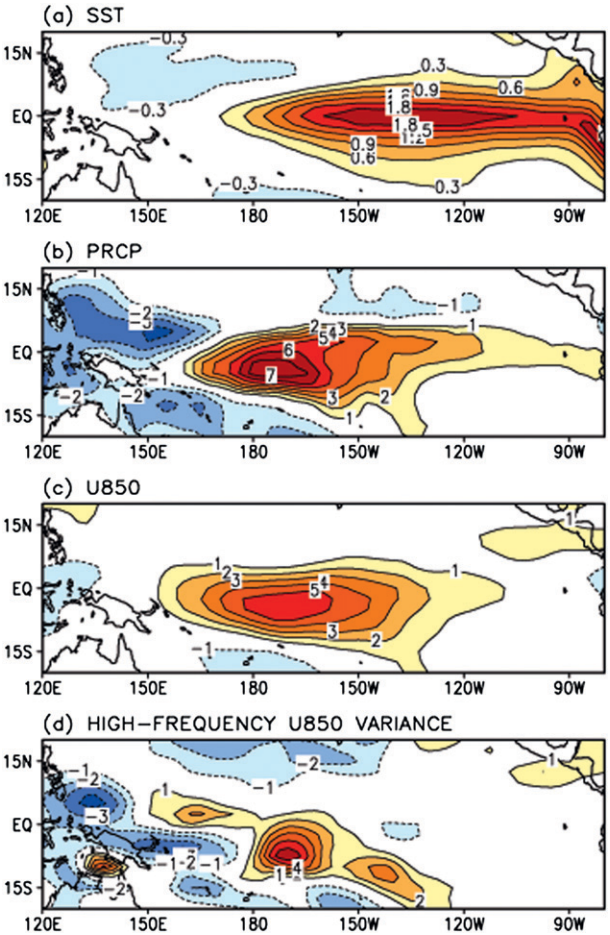

FIG. 2. Observed DJF (a) SST, (b) precipitation, (c) 850-hPa zonal wind, and (d) high frequency 850-hPa zonal-wind variance anomalies during El Niño. Note that five El Niño events, including the 1982/83, 1986/87, 1991/92, 1994/95, and 1997/98 events, are the same as those for obtaining prescribed SST for the ElSST run. A 2–90-day Lanczos bandpass filter (using 45 weights) is applied to the daily mean zonal-wind anomalies at the 850-hPa level; then the DJF HF wind variability, averaged over the El Niño events, is subtracted from that averaged over the DJF season of the whole year to obtain the anomalous seasonal-mean HF wind variability related to El Niño.

of the LF zonal wind and meridional shear of the LF zonal wind. The dominance of EKE generation by these terms was consistent with barotropic wave accumulation by the mean flow, as has been noted in several studies (Holland 1995; Webster and Chang 1988; Sobel and Bretherton 1999). Their results are consistent with Sooraj et al. (2009), who show that enhanced HF zonal-wind variability is closely related to the LF horizontal wind shear as well as vertical wind shear.

To check whether our AGCM can simulate realistic state-dependent HF zonal-wind variability, the same analysis is applied using two AGCM simulations, namely, the

CliSST run and the ElSST run. Figure 3 shows the difference of 30-yr averaged SST, precipitation, and 850-hPa zonal wind between the two simulations, ElSST run minus CliSST run. To the first order the overall difference features are similar to those observed. For example, the simulated central Pacific precipitation and zonal-wind anomalies during El Niño have a similar location and spatial structure to the observations. However, the positive precipitation anomalies in the model simulation are narrower, shifted to the west, and more meridionally symmetric about the equator than the observations. Further, the model produces unrealistic negative precipitation anomalies in the Northern Hemisphere. The South Pacific convergence zone (SPCZ) related precipitation anomalies are not simulated by the AGCM. In addition, the maximum location of the low-level zonal-wind anomalies in the AGCM simulation is somewhat shifted southwestward than that of the observations.

The spatial pattern of simulated difference of the HF zonal-wind variance between the ElSST and CliSST runs, representing the anomalous HF zonal-wind variance during El Niño events, is similar to that of the observations to a large extent. Figure 4 shows the difference of 30-yr averaged HF zonal-wind variance in the two runs, ElSST minus CliSST, and ime series of the total HF zonal-wind variance in the ElSST run over the central Pacific (15°S–15°N, 160°E–120°W). The enhanced (weaker) HF zonal-wind variance appears east (west) of the date line, which is the east (west) part of the LF 850-hPa zonal-wind maximum (Fig. 3c).

As Sooraj et al. (2009) pointed out, the anomalous low-level LF westerly provides a favorable condition for strong HF zonal-wind variability due to LF easterly vertical shear and horizontal wind convergence. In particular, they showed that HF zonal-wind variance is further enhanced in the eastern part of the LF westerlies, as Seiki and Takayabu (2007a) argued. In this regard, our simulated HF zonal-wind variability is quite similar to the observed (Fig. 2d), even though the model simulates a southward-shifted anomalous dipole structure of the HF wind variance with a positive maximum at 15°S. This implies that this AGCM has the ability to simulate state-dependent HF zonal-wind variability during the selected El Niño events.

Interestingly, the magnitude of HF zonal-wind variance varies significantly in time with fixed boundary conditions. It means that the HF zonal-wind variability can be internally modulated via atmospheric processes regardless of the SST boundary condition. It will be quite interesting to examine how the modulation of HF zonal-wind variability is linked to the LF atmospheric state. To investigate the LF atmospheric fields related to internal modulation of the HF zonal-wind variance, a composite analysis based on the box-averaged (15°S–15°N, 160°E–120°W) HF zonal-wind variance, as shown in Fig. 4b, is performed. Among 120 samples (4 seasons × 30 years), events for the strong (weak) HF zonal-wind variance are selected when the box-averaged anomalous HF zonal-wind variance is stronger (weaker) than its standard deviation.

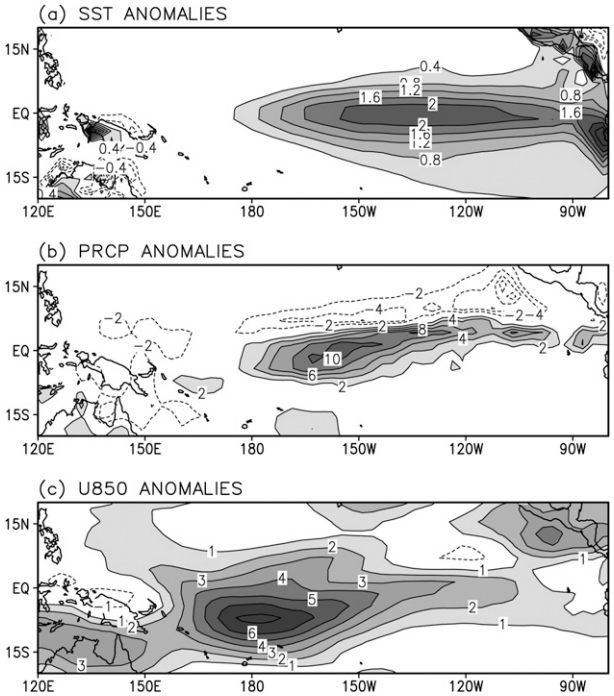

FIG. 3. The difference of 30-yr averaged (a) SST (K), (b) precipitation (mm day^{-1}), and (c) 850-hPa zonal-wind anomalies (m s^{-1}) between the ElSST and CliSST runs.

Figure 5 shows the anomalous HF zonal-wind variance, LF zonal wind at 850 hPa, and precipitation anomalies during the strong HF zonal-wind variance period in the ElSST run. Note that the anomaly in Fig. 5 is defined by the deviation from 30-yr averaged climatology in the ElSST run. Hereafter, analyses using model output are only shown, and some of observational evidence about the key argument in this paper will be discussed in section 4.

As expected, the positive anomaly of HF zonal-wind variance occurs over the equatorial central Pacific. This positive maximum of the anomalous HF zonal-wind variance is slightly shifted to the south of the equator. Similar to the spatial pattern of anomalous HF zonal-wind variance, there is an anomalous low-level LF westerly over the equatorial central Pacific with a slight shift to the south. In addition, the strong HF zonal-wind variance is slightly shifted to the east compared to that of the LF zonal-wind anomalies, consistent with Seiki and Takayabu (2007a) and Sooraj et al. (2009). On the other hand, it is interesting that the precipitation anomaly for

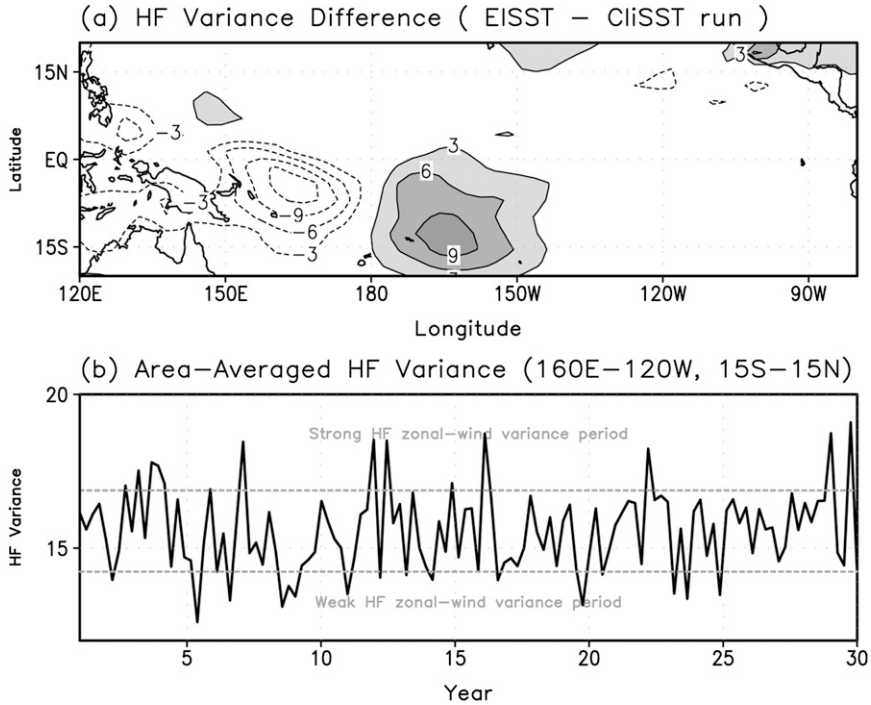

FIG. 4. Simulation results of the (a) high frequency 850-hPa zonal-wind variance with DJF El Niño SST anomalies and (b) box-averaged (15°S–15°N, 160°E–120°W) HF variance in the ElSST run. Upper (lower) dotted line in (b) denotes the criterion for strong (weak) HF zonal-wind variance period.

the period with strong HF zonal-wind variance is negative over the equatorial central Pacific, which is quite different from the El Niño responses shown in Figs. 2 and 3. If the LF westerly anomalies are induced by a precipitation anomaly, there should be a positive precipitation anomaly over the LF westerly anomalies because of the in-phase relation between positive convection LF westerly anomalies over the tropics on interannual time scales (Clarke 1994). However, the composites in Fig. 5 show opposite signs of precipitation and LF zonal-wind anomalies over the south-central Pacific, implying that the anomalous LF westerlies are not generated from the equatorial precipitation anomalies.

On one hand, the atmospheric heating (i.e., precipitation anomaly) induces the LF winds; on the other hand, LF winds can induce precipitation—meaning that the anomalous LF westerlies can induce negative equatorial precipitation anomalies because equatorial westerlies induce low-level divergence due to frictional Ekman pumping (Holton 2004). The LF wind anomaly over the central Pacific has a maximum around 5°S, 160°W. It generates a positive vorticity anomaly between 5°S and 0° and negative vorticity anomaly below that latitude. The secondary circulation due to the positive vorticity over the Southern Hemisphere induces descending motion (brown dots in Fig. 5b), accompanied by the negative precipitation anomaly. On the other, the secondary circulation due to the negative vorticity generates ascending motion over the Southern Hemisphere (green dots in Fig. 5b). this is consistent with the dipole pattern of precipitation anomalies, which shows negative (positive) values at 5°S (10°S) over the central Pacific. Note that the upward secondary circulation is not well matched to the precipitation anomaly over the Northern Hemisphere, possibly due to the relatively weak climatological precipitation over the Northern Hemisphere during DJF. This implies that precipitation anomalies are actually in response to the LF winds. If this process works, then we should ask what leads to the LF westerly anomalies, which are not directly in response to precipitation-induced diabatic heating.

We suggest here that the strong HF variance can contribute to LF westerlies because the HF zonal wind is positively skewed and westerly events are stronger and more frequent than easterly events; therefore, the long-term mean for sequential HF events can generate the westerly residual. Once LF westerlies are induced, they can enhance HF zonal-wind variability further because the LF zonal wind provides a favorable condition for stronger HF zonal-wind variability, leading to intensified LF westerlies. Such two-way interaction between the HF

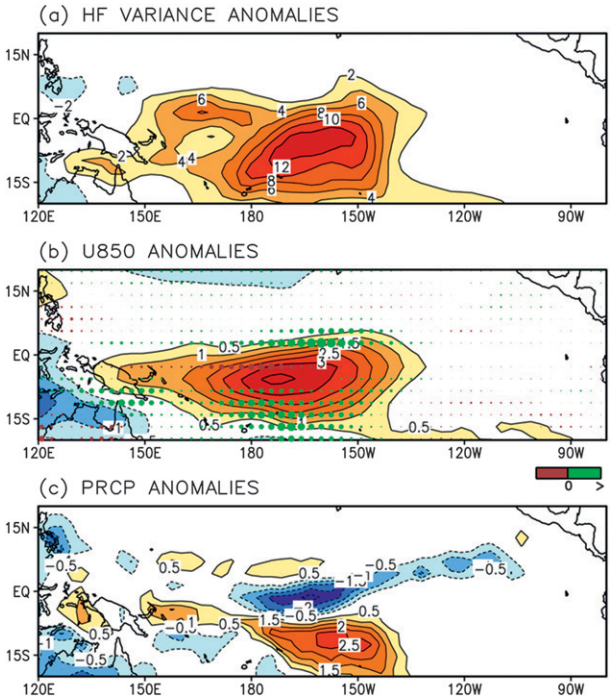

FIG. 5. (a) HF wind variance, (b) LF 850-hPa zonal wind, and (c) precipitation anomalies in the strong HF activity period composite in the ElSST run. LF is defined as 3-month averaged anomaly values. Note that the definition of anomaly in this figure is the difference of seasonal-mean values from the 30-yr averaged climatology in the ElSST run. The green dots in (b) denote Ekman pumping derived by 850-hPa winds [i.e., $f^{-1}(\partial v/\partial x - \partial u/\partial y)$]. The dark (light) shading are related to the secondary downward (upward) motion. For simplicity, we ignore the latitudinal variation of f.

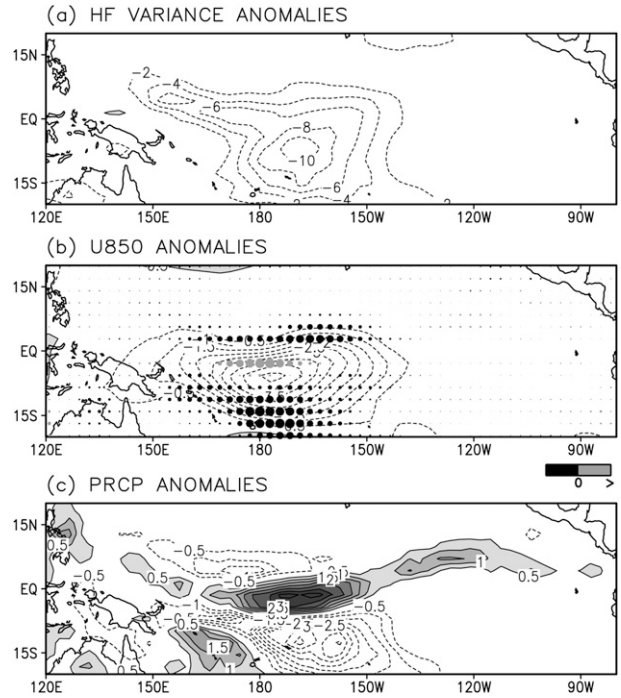

FIG. 6. As in Fig. 5 but in the weak HF activity period composite in the ElSST run. The black (gray) dots in (b) are related to the secondary downward (upward) motion.

zonal-wind variability and LF winds may produce strong internal variability as seen in Fig. 4b.

Figure 6 shows the anomalous HF zonal-wind variance, LF zonal wind at 850 hPa, and precipitation anomalies during the weak HF zonal-wind variance period. Even though the strong and weak absolute magnitudes of the HF zonal-wind variance are not equal, their overall spatial structures along with those of the LF zonal-wind anomalies are quite similar. For instance, there is a negative anomaly of HF zonal-wind variance over the equatorial central Pacific and the LF zonal-wind anomaly is easterly with a maximum over the equatorial central Pacific. Opposite to the strong HF zonal-wind variance composite, the precipitation anomaly over the equatorial region is positive and cannot lead the negative LF zonal-wind anomaly. This indicates that the secondary circulation in controlling internal HF zonal-wind variability and LF zonal wind works similarly for both strong and weak HF zonal-wind variance periods.

Until now, we have shown that, during strong (weak) HF zonal-wind variance periods over the equatorial central Pacific, a LF westerly (easterly) anomaly exists over that region. This supports a positive relationship between the LF zonal wind and HF zonal-wind variance over the equatorial central Pacific. To investigate further the relationship between the LF zonal wind and HF zonal-wind variance, Fig. 7 shows the correlation coefficients between the 850-hPa LF zonal-wind anomaly and anomalous 850-hPa HF zonal-wind variance. In Figs. 7a and 7b, the values with 95% confidence level using a two-tailed Student's t test are shaded. Note that the correlation coefficients represent the relationship for internal variability regardless of the SST condition. Consistent with previous results, the positive correlation coefficient over the equatorial central Pacific is significant in the ElSST run. Similarly, the positive correlation between the LF zonal wind and HF zonal-wind variance is large over the equatorial central-eastern Pacific and northwestern-central Pacific in the CliSST run. In addition to the equatorial central Pacific, high positive correlation is seen over the off-equatorial southeastern Pacific around 120°W and over the northwestern Pacific near 150°E. On the other hand, there are negative correlation coefficients of about −0.3 over the off-equatorial southwestern Pacific and far-eastern Pacific.

The overall correlation pattern in the CliSST run is similar to that of the ElSST run; however, the positive

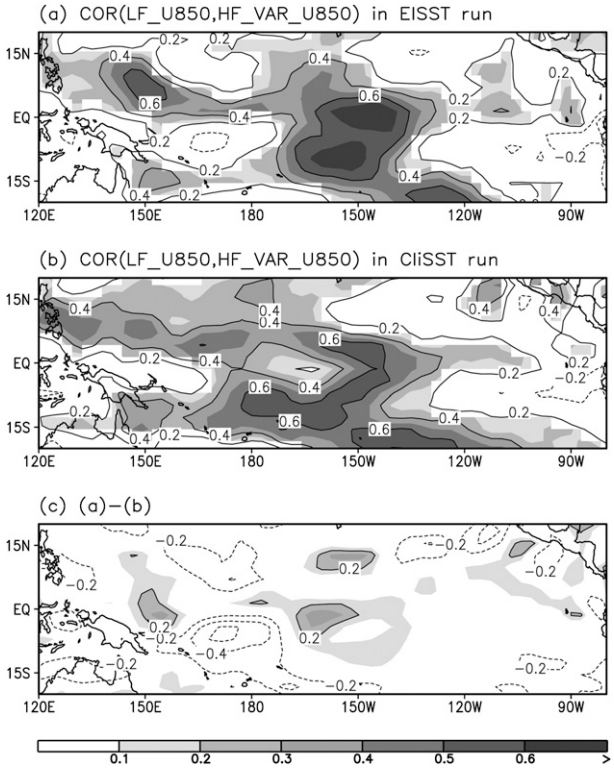

FIG. 7. (a),(b) Correlation coefficients between the LF 850-hPa zonal-wind anomaly and HF wind variance at 850 hPa in both experiments: values at the 95% confidence level shaded. (c) Difference between the ElSST and CliSST run.

correlation over the off-equatorial southern Pacific is extended to the west. Therefore, the negative correlation over the off-equatorial southwestern Pacific is not as large as that in the ElSST run. The difference map between the correlation in the ElSST run and that in the CliSST run shows a negative correlation difference over the south- and north-central Pacific around 170°E. The positive correlation difference over the central Pacific is also shown. We will discuss in more detail what causes these differences in spatial pattern between the two experiments.

Based on the high correlation between the LF zonal-wind anomaly and anomalous HF zonal-wind variance, one can argue that the significant correlation between the LF zonal-wind anomaly and anomalous HF zonal-wind variance is robust because of the role of the LF zonal wind on HF zonal-wind variability, as already mentioned in several studies (Kug et al. 2009c; Sooraj et al. 2009). However, if the anomalous HF zonal-wind variance is solely generated by the LF zonal-wind anomaly, the negative correlation over the far-eastern and off-equatorial southwestern Pacific is hard to explain. Note that the anomalous LF westerly (easterly) only enhances (reduces) HF zonal-wind variance; therefore, the negative relationship between the LF zonal wind and HF zonal-wind variance can be led by the rectification process of HF zonal-wind events on the LF zonal wind.

As suggested earlier, an asymmetric HF zonal wind can contribute to the LF zonal wind by the rectification process. For example, wherever a westerly phase of the HF zonal wind is more dominant than the easterly phase of HF zonal wind (e.g., positively skewed HF zonal wind), enhanced HF zonal-wind variance leads to generation of a rectified LF westerly. Similarly, we can expect that the enhanced HF zonal-wind variance may lead to anomalous LF easterlies if anomalous HF zonal wind is negatively skewed. Therefore, it is worthwhile to investigate whether the correlation between HF zonal-wind variance and the LF zonal wind is associated with the skewness of anomalous HF zonal wind.

To investigate the asymmetry of anomalous HF zonal wind, skewness is introduced (Trenberth 1997; Burgers and Stephenson 1999; Hannachi et al. 2003; Jin et al. 2003; An and Jin 2004; An et al. 2005). The moment coefficient of skewness is defined by the normalized third statistical moment as follows:

$$\text{skewness} = \frac{m_3}{(m_2)^{3/2}},$$

where m_k is the kth moment,

$$m_k = \sum_{i=1}^{N} \frac{(x_i - \overline{X})^k}{N}$$

in which x_i is the ith data of HF wind anomaly, $\overline{X}$ is the mean of HF wind, and N is the number of samples (30 yr × 365 days = 10 950 samples).

Figure 8 shows the climatological (i.e., 30 yr averaged) skewness of the anomalous HF zonal wind in both simulations. In these simulations, overall climatological skewness is positive over the Pacific region, indicating more frequent strong anomalous HF westerly events. This is consistent with the observations (not shown). In addition, this figure is consistent with Fig. 6 of Philip and van Oldenborgh (2009), even though positive skewness is more confined to the western Pacific in their study. In the ElSST run, positive skewness is over the central Pacific, off-equatorial central-eastern Pacific around 120°W, and northwestern Pacific. In contrast, there is weak negative skewness over the far-eastern Pacific. The overall pattern of climatological skewness in the CliSST run is similar to that in the ElSST run; however, positive skewness over the off-equatorial southern Pacific is extended to the west compared to that in the ElSST run. Therefore, there is negative skewness difference between the ElSST

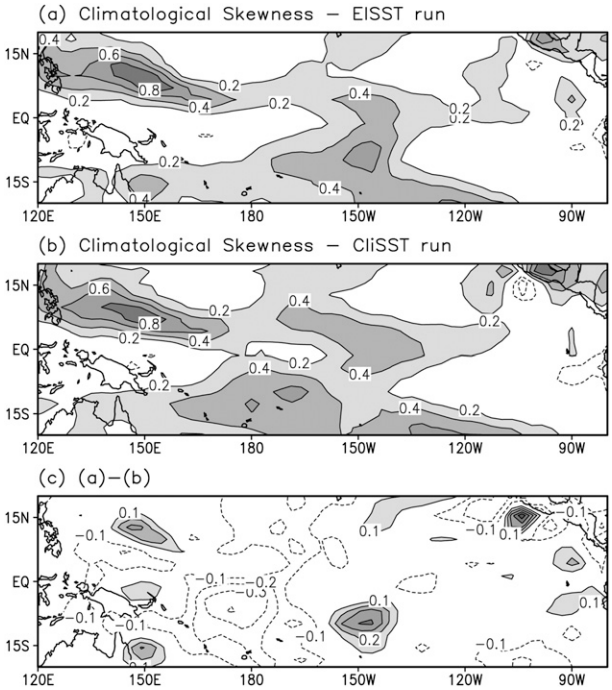

FIG. 8. (a),(b) Climatological skewness of high-pass-filtered 850-hPa zonal winds in both experiments. (c) Difference between the ElSST and CliSST runs.

run and CliSST run around 170°E; whereas there is a positive skewness difference over the central Pacific around 10°S, 150°W.

Surprisingly, it is found that the spatial pattern of climatological skewness of anomalous HF zonal wind exhibits a similarity to that of the correlation map between the LF zonal-wind anomaly and anomalous HF zonal-wind variance, as shown in Fig. 7. Over the positive skewness regions of anomalous HF zonal wind (e.g., the central Pacific), enhanced HF zonal-wind variance induces an additional residual LF westerly; therefore, there is positive correlation between HF zonal-wind variance and the LF zonal wind. On the other hand, over the negative skewness regions, like the far-eastern Pacific, enhanced HF zonal-wind variance induces an additional LF easterly; therefore, it leads to a negative correlation between HF zonal-wind variance and LF zonal wind. In addition, the difference in the correlation map between the LF zonal-wind anomaly and anomalous HF zonal-wind variance between the two runs is also clearly reflected in the difference of climatological skewness of anomalous HF zonal wind. For example, the westward extension of positive anomaly of climatological HF zonal-wind skewness over the off-equatorial southwestern Pacific in the CliSST run is well matched to that of the correlation between anomalous HF zonal-wind variance and LF zonal-wind anomaly. Therefore, it is possible that the rectification process due to the asymmetry of HF zonal-wind events can generate additional LF zonal wind.

To investigate the similarity of spatial patterns between the correlation map (between the LF zonal-wind anomaly and anomalous HF zonal-wind variance, Fig. 7) and climatological skewness of HF zonal-wind variance (Fig. 8), the scatter diagram between the correlation and climatological HF zonal-wind skewness over the equatorial Pacific region (10°S–10°N, 120°E–90°W) is shown in Fig. 9. As mentioned earlier, there is a clear linear relationship between the two. The pattern correlation coefficients between the two maps are 0.87 (0.92) in the ElSST (CliSST) run. It means that the correlation between the LF zonal-wind anomaly and anomalous HF zonal-wind variance strongly depends on the skewness of HF zonal wind because the positive anomaly of HF zonal-wind variance generates positive (negative) residuals of LF zonal wind under positive (negative) HF zonal-wind skewness.

If only a one-way process from the LF zonal wind to HF zonal-wind variance is robust (e.g., LF zonal-wind modulates HF zonal-wind variance; therefore, fluctuations of HF zonal-wind variance are solely from that of LF zonal wind), the correlation coefficients between the LF zonal-wind anomaly and anomalous HF zonal-wind variance would be independent of skewness of the HF zonal wind. For example, if the fluctuation of HF zonal-wind variance is a result of that of LF zonal wind, HF zonal-wind variance would be enhanced (weakened) by LF westerlies (easterly) regardless of the sign of the HF zonal-wind skewness. This means, if the one-way process from LF zonal wind to HF zonal-wind variance is dominant, the correlation between the LF zonal-wind anomaly and anomalous HF zonal-wind variance would be positive even over the negative skewness region. Therefore, negative correlation coefficients clearly mean that there is an upscaling feedback process that the residual of HF zonal-wind variability induces the LF zonal wind.

To further confirm that the asymmetry of anomalous HF zonal wind leads to the residual LF zonal wind, Fig. 10a shows the probability distribution functions (PDFs) of total daily-mean zonal wind at 850 hPa over the central Pacific (15°S–15°N, 160°E–120°W) in the ElSST run. Consistent with the definition, the PDF for strong (weak) HF zonal-wind variance period is broader (narrower) than PDFs in other cases. As the PDF is broader, the largest peak probability is reduced for the strong HF zonal-wind variance period. For example, the peak of the PDF for a normal HF zonal-wind variance period is about 0.04; however, it is reduced to less than 0.035 for a strong HF zonal-wind variance period. Instead, there is a significant increase of the PDF for extreme values, especially

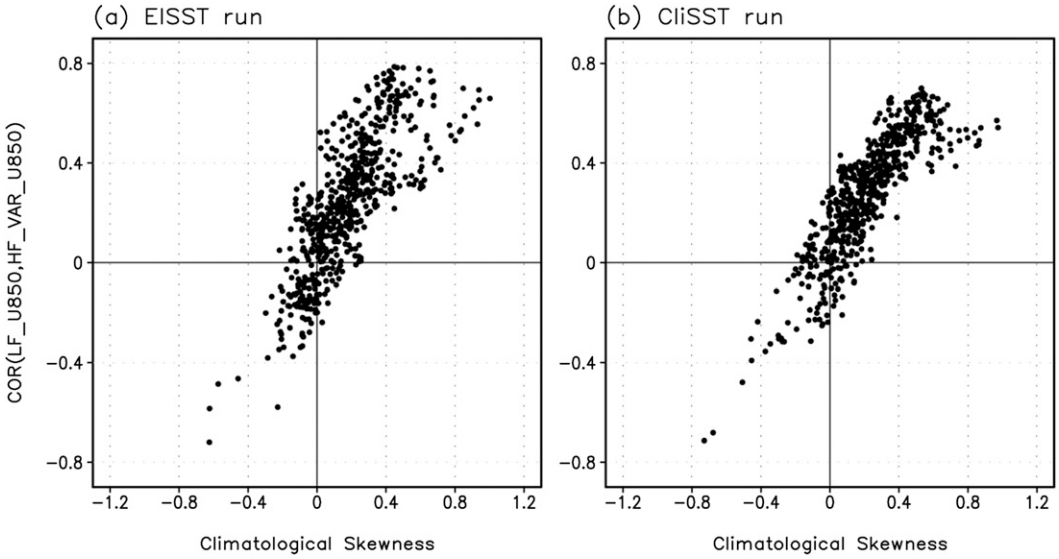

FIG. 9. (a),(b) Scatter diagram of the climatological skewness of high-pass filtered 850-hPa zonal wind vs correlation coefficients between LF 850-hPa zonal wind anomaly and HF wind variance at 850 hPa over equatorial Pacific regions (10°S–10°N, 120°E–90°W) in both experiments.

for high extreme values because of the positive asymmetry of HF zonal wind.

In addition, it is interesting that the value with maximum PDF is relatively high in the strong HF zonal-wind variance period compared to that in the weak HF zonal-wind variance period. This might be due to the LF westerly zonal wind increasing the HF zonal-wind variance (Kug et al. 2009c), which emphasizes the role of the LF zonal wind on HF zonal-wind variance. Or, this might be due to the additional LF zonal wind generated by the rectification of the asymmetric HF zonal wind. This mean shift of the PDF affects the probability of HF westerly/easterly events. Because we are focusing on the rectification process, we try to exclude the impact of the LF zonal wind on HF wind events by removing the median value of the PDF for each case. The median value is used because rectification of the HF wind on LF wind is already reflected in the mean value.

Figure 10b shows the PDF of the daily-mean zonal wind after subtracting the median value. In addition, Fig. 10c shows the probability of anomalous HF westerly/easterly events for weak, normal, and strong HF zonal-wind variance periods. Note that the anomalous HF westerly and easterly events are defined when the median-shifted

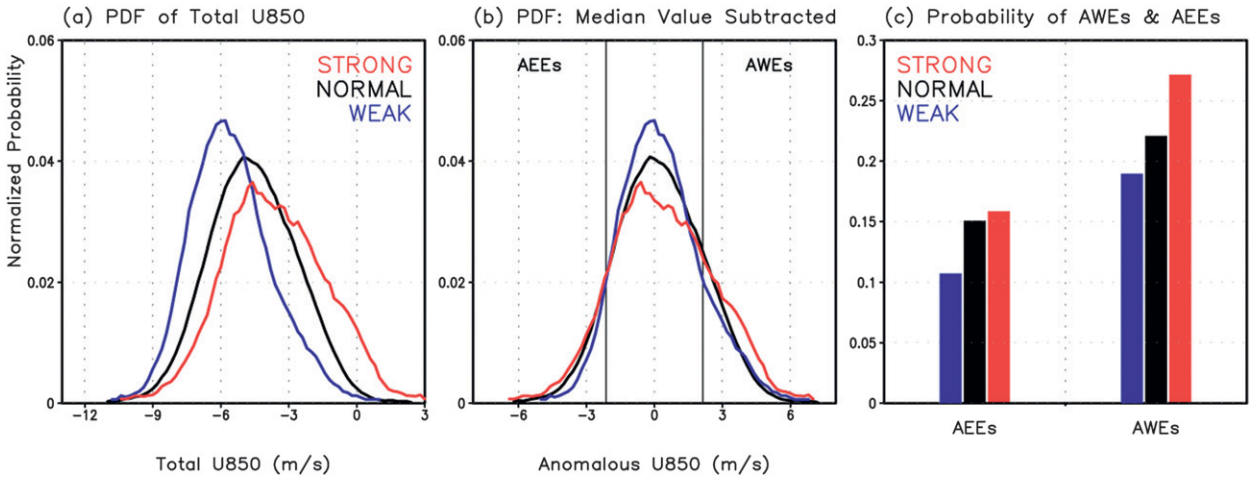

FIG. 10. PDF of (a) daily total zonal winds at 850 hPa over the central Pacific (15°S–15°N, 160°E–120°W) and (b) with the median value subtracted. (c) Probability of AEWs and AEEs for weak, normal, and strong HF activity periods in the ElSST run.

daily-mean 850-hPa zonal wind in Fig. 10b is greater and smaller than 1 (−1) standard deviation, respectively. For simplicity, the anomalous HF westerly and easterly events are referred to as anomalous westerly events (AWEs) and anomalous easterly events (AEEs). This definition does not consider the duration of wind events, which is somewhat different from the conventional way that wind events are chosen such as when the wind values remain above the criteria for several days. However, most selected AWEs (or AEEs) persist at least several days (not shown); therefore, the major conclusion will not be not changed even though the definition of wind events is slightly different.

Because the PDF in Fig. 10b becomes broader for the strong HF zonal-wind variance period than that for the weak HF zonal-wind variance period, the probability for both AWEs and AEEs is increased. Between the AWEs and AEEs, the increase of AWEs is excessive because of the positive asymmetric nature of HF zonal wind. For example, the difference between the probability of AWEs from that of AEEs is 0.07 in the weak HF zonal-wind variance period, while it is increased to 0.11 in the strong HF zonal-wind variance period. This means that the increase of HF zonal-wind variance increases AWEs more than AEEs; therefore, the mean (or LF) zonal wind for the strong zonal-wind variance period is also increased.

4. Summary and discussion

In this study, the process of HF zonal-wind variability rectification of the LF zonal wind is investigated using the two idealized AGCM experiments. Because observed and simulated HF wind anomalies are positively skewed, enhanced HF zonal-wind variance generates an additional residual LF westerly anomaly. This conclusion is supported by the result that high positive correlation coefficients between HF zonal-wind variance and the LF zonal wind are only found over the positive HF zonal-wind skewness region, while there is negative correlation over the negative HF zonal-wind skewness region. For example, if the HF westerly anomaly is much stronger than the HF easterly anomaly, the enhanced HF zonal-wind variance can produce a residual westerly anomaly; however, if the magnitude of HF westerly anomalies is the same as that of HF easterly anomalies (i.e., weak or negative skewness of anomalous HF zonal wind), there would be no (or negligible) residual LF zonal wind.

One may wonder how robust this rectified process is in the observations. To investigate this, the authors applied a similar analysis to the observational data and concluded that a similar rectified process is at work in the observations to some extent. For example, the scatter diagram between HF and LF correlation and climatological skewness of HF zonal wind is linear in the equatorial Pacific (10°S–10°N, 120°E–90°W), and the correlation coefficient between them is 0.54 at the 99% significance level. For example, negative climatological skewness is not shown over the regions of negative correlation. This lower correlation in observations compared to the simulation may be due to the LF zonal wind generated by time-varying SST in the observations; therefore, generation of the LF zonal wind due to SST forcing is confounded with that due to the rectification process (i.e., HF–LF interaction within the atmospheric system).

Rectification of HF zonal wind also might lead to eastward propagation of LF zonal-wind anomalies because the HF zonal-wind variance is enhanced over the eastern part of LF zonal wind (Seiki and Takayabu 2007a; Sooraj et al. 2009). Once LF westerlies are generated, they leads to stronger HF zonal-wind variance, especially over the eastern part of the LF westerly wind. Then, enhanced HF zonal-wind variance reinforces the LF westerly due to the positive asymmetry of the HF zonal wind only over the eastern part of the LF westerly; therefore, the center of LF westerlies is moved to the east. Then, the reinforced LF westerly generates enhanced HF zonal-wind variance over the eastern part of the LF westerly.

Even though the current experimental design is easy to exclude the impact of SST-forced LF winds, it has drawbacks because the seasonal dependency of the HF–LF relationship cannot be considered. According to previous studies (Hendon et al. 2007; Gushchina and Dewitte 2011), interaction between ENSO and MJO is also robust during boreal spring; however, the HF–LF relation is strongest during boreal winter, possibly due to the increase of synoptic-scale wind variability (Sokolikhina et al. 2006). In addition, there is the possibility that the degree of the HF–LF relationship can be different when the SST forcing is changed to the boreal spring season. Therefore, it will be quite interesting to examine the seasonal dependency of rectification feedback on the HF–LF wind interaction. The simple model experimental design, presented here, will be also quite useful for further study.

Acknowledgments. This work was supported by the National Research Foundation of Korea (Grant NRF-2009-C1AAA001-2009-0093042), funded by the Korean government (MEST).

REFERENCES

An, S.-I., and F.-F. Jin, 2004: Nonlinearity and asymmetry of ENSO. *J. Climate,* **17,** 2399–2412.

——, Y.-G. Ham, J.-S. Kug, F.-F. Jin, and I.-S. Kang, 2005: El Niño–La Niña asymmetry in the Coupled Model Intercomparison Project simulations. *J. Climate,* **18,** 2617–2627.

——, J.-S. Kug, Y.-G. Ham, and I.-S. Kang, 2008: Successive modulation of ENSO to the future greenhouse warming. *J. Climate,* **21,** 3–21.

Ashok, K., S. K. Behera, S. A. Rao, H. Weng, and T. Yamagata, 2007: El Niño Modoki and its possible teleconnection. *J. Geophys. Res.,* **112,** C11007, doi:10.1029/2006JC003798.

Batstone, C., and H. H. Hendon, 2005: Characteristics of stochastic variability associated with ENSO and the role of the MJO. *J. Climate,* **18,** 1773–1789.

Blaauboer, D., G. J. Komen, and J. Reiff, 1982: The behaviour of the sea surface temperature (SST) as a response to stochastic latent- and sensible heat forcing. *Tellus,* **34,** 17–28.

Bonan, G. B., 1996: A land surface model (LSM version 1.0) for ecological, hydrological, and atmospheric studies: Technical description and user's guide. NCAR Tech. Note NCAR/TN-417+STR, 150 pp.

Burgers, G., and D. B. Stephenson, 1999: The "normality" of El Niño. *Geophys. Res. Lett.,* **26,** 1027–1030.

Clarke, A. J., 1994: Why are surface equatorial ENSO winds anomalously westerly under anomalous large-scale convection? *J. Climate,* **7,** 1623–1627.

Duchon, C., 1979: Lanczos filtering in one and two dimensions. *J. Appl. Meteor.,* **18,** 1016–1022.

Eisenman, I., L. Yu, and E. Tziperman, 2005: Westerly wind bursts: ENSO's tail rather than the dog? *J. Climate,* **18,** 5224–5238.

Fink, A., and P. Speth, 1997: Some potential forcing mechanisms of the year-to-year variability of the tropical convection and its intraseasonal (25-70-day) variability. *Int. J. Climatol.,* **17,** 1513–1534.

Gebbie, G., I. Eisenman, A. Wittenberg, and E. Tziperman, 2007: Modulation of westerly wind bursts by sea surface temperature: A semistochastic feedback for ENSO. *J. Atmos. Sci.,* **64,** 3281–3295.

Gushchina, D., and B. Dewitte, 2011: The relationship between intraseasonal tropical variability and ENSO and its modulation at seasonal to decadal timescales. *Cent. Eur. J. Geosci.,* **3,** 175–196, doi:10.2478/s13533-011-0017-3.

Han, W., P. Webster, R. Lukas, P. Hacker, and A. Hu, 2004: Impact of atmospheric intraseasonal variability in the Indian Ocean: Low-frequency rectification in equatorial surface current and transport. *J. Phys. Oceanogr.,* **34,** 1350–1372.

Hannachi, A., D. Stephenson, and K. Sperber, 2003: Probability-based methods for quantifying nonlinearity in the ENSO. *Climate Dyn.,* **20,** 241–256.

Harrison, D. E., and P. S. Schopf, 1984: Kelvin-wave-induced anomalous advection and the onset of surface warming in El Niño events. *Mon. Wea. Rev.,* **112,** 923–933.

——, and G. A. Vecchi, 1997: Westerly wind events in the tropical Pacific, 1986–95. *J. Climate,* **10,** 3131–3156.

Hendon, H. H., and M. C. Wheeler, 2008: Some space–time spectral analyses of tropical convection and planetary-scale waves. *J. Atmos. Sci.,* **65,** 2936–2948.

——, ——, and C. Zhang, 2007: Seasonal dependence of the MJO–ENSO relationship. *J. Climate,* **20,** 531–543.

Holland, G., 1995: Scale interaction in the western Pacific monsoon. *Meteor. Atmos. Phys.,* **56,** 57–79.

Holton, J. R., 2004: *An Introduction to Dynamic Meteorology*. 4th ed. Academic Press, 535 pp.

Holtslag, A. A. M., and B. A. Boville, 1993: Local versus nonlocal boundary-layer diffusion in a global climate model. *J. Climate,* **6,** 1825–1842.

Huffman, G. J., R. F. Adler, M. M. Morrissey, D. T. Bolvin, S. Curtis, R. Joyce, B. McGavock, and J. Susskind, 2001: Global precipitation at one-degree daily resolution from multisatellite observations. *J. Hydrometeor.,* **2,** 36–50.

Jin, F.-F., S.-I. An, A. Timmermann, and J. Zhao, 2003: Strong El Niño events and nonlinear dynamical heating. *Geophys. Res. Lett.,* **30,** 1120, doi:10.1029/2002GL016356.

——, L. Lin, A. Timmermann, and J. Zhao, 2007: Ensemble-mean dynamics of the ENSO recharge oscillator under state-dependent stochastic forcing. *Geophys. Res. Lett.,* **34,** L03807, doi:10.1029/2006GL027372.

Kalnay, E., and Coauthors, 1996: The NCEP/NCAR 40-Year Reanalysis Project. *Bull. Amer. Meteor. Soc.,* **77,** 437–471.

Kao, H.-Y., and J.-Y. Yu, 2009: Contrasting eastern-Pacific and central-Pacific types of ENSO. *J. Climate,* **22,** 615–632.

Kessler, W. S., and R. Kleeman, 2000: Rectification of the Madden–Julian oscillation into the ENSO cycle. *J. Climate,* **13,** 3560–3575.

——, M. J. McPhaden, and K. M. Weickmann, 1995: Forcing of intraseasonal Kelvin waves in the equatorial Pacific. *J. Geophys. Res.,* **100** (C6), 10 613–10 631.

Kim, D., J.-S. Kug, I.-S. Kang, F.-F. Jin, and A. T. Wittenberg, 2008: Tropical Pacific impacts of convective momentum transport in the SNU coupled GCM. *Climate Dyn.,* **31,** 213–226.

——, and Coauthors, 2009: Application of MJO simulation diagnostics to climate models. *J. Climate,* **22,** 6413–6436.

Kirtman, B. P., K. Pegion, and S. Kinter, 2005: Internal atmospheric dynamics and tropical Indo-Pacific climate variability. *J. Atmos. Sci.,* **62,** 2220–2233.

Kraus, E. B, and J. S. Turner, 1967: A one-dimensional model of the seasonal thermocline II. The general theory and its consequences. *Tellus,* **19,** 98–106.

Kug, J.-S., and Y.-G. Ham, 2011: Are there two types of La Nina events? *Geophys. Res. Lett.,* **38,** L16704, doi:10.1029/2011GL048237.

——, F.-F. Jin, K. P. Sooraj, and I.-S. Kang, 2008a: State-dependent atmospheric noise associated with ENSO. *Geophys. Res. Lett.,* **35,** L05701, doi:10.1029/2007GL032017.

——, I.-S. Kang, and D.-H. Choi, 2008b: Seasonal climate predictability with tier-one and tier-two prediction systems. *Climate Dyn.,* **31,** 403–416, doi:10.1007/s00382-007-0264-7.

——, F.-F. Jin, and S.-I. An, 2009a: Two types of El Niño events: Cold tongue El Niño and warm pool El Niño. *J. Climate,* **22,** 1499–1515.

——, K. P. Sooraj, F.-F. Jin, J.-J. Luo, and M.-H. Kwon, 2009b: Impact of Indian Ocean dipole on high-frequency atmospheric variability over the Indian Ocean. *Atmos. Res.,* **94,** 134–139.

——, ——, D. Kim, I.-S. Kang, F.-F. Jin, Y. N. Takayabu, and M. Kimoto, 2009c: Simulation of state-dependent high-frequency atmospheric variability associated with ENSO. *Climate Dyn.,* **32,** 635–648.

——, M.-S. Ahn, M.-K. Sung, S.-W. Yeh, H.-S. Min, and Y.-H. Kim, 2010a: Statistical relationship between two types of El Niño events and climate variation over the Korean Peninsula. *Asia-Pac. J. Atmos. Sci.,* **46,** 467–474.

——, J. Choi, S.-I. An, F.-F. Jin, and A. T. Wittenberg, 2010b: Warm pool and cold tongue El Niño events as simulated by the GFDL 2.1 coupled GCM. *J. Climate,* **23,** 1226–1239.

——, K.-P. Sooraj, T. Li, and F.-F. Jin, 2010c: Precursors of El Niño/La Niña onset and their interrelationship. *J. Geophys. Res.,* **115,** D05106, doi:10.1029/2009JD012861.

Lau, K., and N. Lau, 1992: The energetics and propagation dynamics of tropical summertime synoptic-scale disturbances. *Mon. Wea. Rev.,* **120,** 2523–2539.

Lee, M., I.-S. Kang, J. Kim, and B. Mapes, 2001: Influence of cloud-radiation interaction on simulating tropical intraseasonal oscillation with an atmospheric general circulation model. *J. Geophys. Res.,* **106** (D13), 14 219–14 233.

——, ——, and B. Mapes, 2003: Impacts of cumulus convection parameterization on aqua-planet AGCM simulations of tropical intraseasonal variability. *J. Meteor. Soc. Japan,* **81,** 963–992.

Lengaigne, M., J.-P. Boulanger, C. Menkes, S. Masson, G. Madec, and P. Delacluse, 2002: Ocean response to the March 1997 westerly wind event. *J. Geophys. Res.,* **107,** 8015, doi:10.1029/2001JC000841.

——, E. Guilyardi, J. P. Boulanger, C. Menkes, P. Delecluse, P. Inness, J. Cole, and J. M. Slingo, 2004: Triggering of El Niño by westerly wind events in a coupled general circulation model. *Climate Dyn.,* **23,** 601–620.

Le Treut, H., and Z.-X. Li, 1991: Sensitivity of an atmospheric general circulation model to prescribed SST changes: Feedback effects associated with the simulation of cloud optical properties. *Climate Dyn.,* **5,** 175–187.

Lin, J.-L., and Coauthors, 2006: Tropical intraseasonal variability in 14 IPCC AR4 climate models. Part I: Convective signals. *J. Climate,* **19,** 2665–2690.

McPhaden, M. J., 1999: Genesis and evolution of the 1997-98 El Niño. *Science,* **283,** 950–954.

——, F. Bahr, Y. Dupenhoat, E. Firing, S. P. Hayes, P. Niiler, P. L. Richardson, and J. M. Toole, 1992: The response of the western equatorial Pacific Ocean to westerly wind bursts during November 1989 to January 1990. *J. Geophys. Res.,* **97** (C9), 14 289–14 303.

——, and Coauthors, 1998: The Tropical Ocean-Global Atmosphere observing system: A decade of progress. *J. Geophys. Res.,* **103** (C7), 14 169–14 240.

Moore, A., and R. Kleeman, 1999: Stochastic forcing of ENSO by the intraseasonal oscillation. *J. Climate,* **12,** 1199–1220.

Nakajima, T., M. Tsukamoto, Y. Tsushima, and A. Numaguti, 1995: Modelling of the radiative processes in an AGCM. *Climate System Dynamics and Modelling,* T. Matsuno, Ed., Center for Climate System Research, 104–123.

Numaguti, A., M. Takahashi, T. Nakajima, and A. Sumi, 1995: Development of an atmospheric general circulation model. *Climate System Dynamics and Modelling,* T. Matsuno, Ed., Center for Climate System Research, 1–27.

Perez, C., A. Moore, J. Zavala-Garay, and R. Kleeman, 2005: A comparison of the influence of additive and multiplicative stochastic forcing on a coupled model of ENSO. *J. Climate,* **18,** 5066–5085.

Philip, S. Y., and G. J. van Oldenborgh, 2009: Significant atmospheric nonlinearities in the ENSO cycle. *J. Climate,* **22,** 4014–4028.

Rodgers, K., P. Friederichs, and M. Latif, 2004: Tropical Pacific decadal variability and its relation to decadal modulations of ENSO. *J. Climate,* **17,** 3761–3774.

Seiki, A., and Y. Takayabu, 2007a: Westerly wind bursts and their relationship with intraseasonal variations and ENSO. Part I: Statistics. *Mon. Wea. Rev.,* **135,** 3325–3345.

——, and ——, 2007b: Westerly wind bursts and their relationship with intraseasonal variations and ENSO. Part II: Energetics over the western and central Pacific. *Mon. Wea. Rev.,* **135,** 3346–3361.

Shinoda, T., and H. Hendon, 2002: Rectified wind forcing and latent heat flux produced by the Madden–Julian oscillation. *J. Climate,* **15,** 3500–3508.

Smith, T., and R. Reynolds, 2003: Extended reconstruction of global sea surface temperatures based on COADS data (1854–1997). *J. Climate,* **16,** 1495–1510.

Sobel, A., and C. Bretherton, 1999: Development of synoptic-scale disturbances over the summertime tropical northwest Pacific. *J. Atmos. Sci.,* **56,** 3106–3127.

Sokolikhina, E. V., E. K. Semenov, and N. N. Sokolikhina, 2006: The atmospheric circulation on the synoptic scale during the culmination phase of the El-Niño – Southern Oscillation events (1997–1998). *Adv. Geosci.,* **6,** 17–21.

Sooraj, K., D. Kim, J.-S. Kug, S.-W. Yeh, F.-F. Jin, and I.-S. Kang, 2009: Effects of the low-frequency zonal wind variation on the high frequency atmospheric variability over the tropics. *Climate Dyn.,* **33,** 495–507.

Tiedtke, M., 1983: The sensitivity of the time-mean large-scale flow to cumulus convection in the ECMWF model. *Proc. ECMWF Workshop on Convection in Large-Scale Models,* Reading, United Kingdom, ECMWF, 297–316.

Timmermann, A., and G. Lohmann, 2000: Noise-induced transitions in a simplified model of the thermohaline circulation. *J. Phys. Oceanogr.,* **30,** 1891–1900.

——, F.-F. Jin, and J. Abshagen, 2003: A nonlinear theory for El Niño bursting. *J. Atmos. Sci.,* **60,** 152–165.

Trenberth, K., 1997: The definition of El Niño. *Bull. Amer. Meteor. Soc.,* **78,** 2771–2777.

Vecchi, G. A., and D. E. Harrison, 2000: Tropical Pacific sea surface temperature anomalies, El Niño, and equatorial westerly wind events. *J. Climate,* **13,** 1814–1830.

——, B. J. Soden, A. T. Wittenberg, I. M. Held, A. Leetmaa, and M. J. Harrison, 2006: Weakening of tropical Pacific atmospheric circulation due to anthropogenic forcing. *Nature,* **441,** 73–76.

Waliser, D., K. M. Lau, W. Stern, and C. Jones, 2003: Potential predictability of the Madden–Julian oscillation. *Bull. Amer. Meteor. Soc.,* **84,** 33–50.

Webster, P., and H. Chang, 1988: Equatorial energy accumulation and emanation regions: Impacts of a zonally varying basic state. *J. Atmos. Sci.,* **45,** 803–829.

Weng, H., K. Ashok, S. K. Behera, S. A. Rao, and T. Yamagata, 2007: Impacts of recent El Niño Modoki on dry/wet conditions in the Pacific Rim during boreal summer. *Climate Dyn.,* **29,** 113–129, doi:10.1007/s00382-007-0234-0.

Wheeler, M., and G. N. Kiladis, 1999: Convectively coupled equatorial waves: Analysis of clouds and temperature in the wavenumber–frequency domain. *J. Atmos. Sci.,* **56,** 374–399.

Wu, R., and B. Kirtman, 2006: Changes in spread and predictability associated with ENSO in an ensemble coupled GCM. *J. Climate,* **19,** 4378–4396.

Wu, X., and M. Yanai, 1994: Effects of vertical wind shear on the cumulus transport of momentum: Observations and parameterization. *J. Atmos. Sci.,* **51,** 1640–1660.

Xie, P., and P. Arkin, 1997: Global precipitation: A 17-year monthly analysis based on gauge observations, satellite estimates, and numerical model outputs. *Bull. Amer. Meteor. Soc.,* **78,** 2539–2558.

Yu, L., R. A. Weller, and W. T. Liu, 2003: Case analysis of a role of ENSO in regulating the generation of westerly wind bursts in the western equatorial Pacific. *J. Geophys. Res.,* **108,** 3128, doi:10.1029/2002JC001498.

Zavala-Garay, J., C. Zhang, A. Moore, and R. Kleeman, 2005: The linear response of ENSO to the Madden–Julian oscillation. *J. Climate,* **18,** 2441–2459.

Zhang, C., and J. Gottschalck, 2002: SST anomalies of ENSO and the Madden–Julian oscillation in the equatorial Pacific. *J. Climate,* **15,** 2429–2445.